

# Wind-induced dynamic response and its load estimation for structural frames of single-layer latticed domes with long spans

Yasushi Uematsu<sup>†</sup>, Takayuki Sone<sup>‡</sup> and Motohiko Yamada<sup>††</sup>

*Tohoku University, Sendai 980-8579, Japan*

Takeshi Hongo<sup>‡‡</sup>

*Kajima Technical Research Institute, Chofu, Japan*

*(Received January 16, 2002, Accepted March 22, 2002)*

**Abstract.** The main purpose of this study is to discuss the design wind loads for the structural frames of single-layer latticed domes with long spans. First, wind pressures are measured simultaneously at many points on dome models in a wind tunnel. Then, the dynamic response of several models is analyzed in the time domain, using the pressure data obtained from the wind tunnel experiment. The nodal displacements and the resultant member stresses are computed at each time step. The results indicate that the dome's dynamic response is generally dominated by such vibration modes that contribute to the static response significantly. Furthermore, the dynamic response is found to be almost quasi-static. Then, a series of quasi-static analyses, in which the inertia and damping terms are neglected, is made for a wide range of the dome's geometry. Based on the results, a discussion is made of the design wind load. It is found that a gust effect factor approach can be used for the load estimation. Finally, an empirical formula for the gust effect factor and a simple model of the pressure coefficient distribution are provided.

**Key words:** single-layer latticed dome; wind-induced response; dynamic response analysis; structural frame; load estimation; design wind load; gust effect factor.

---

## 1. Introduction

Single-layer latticed domes are generally light and flexible, compared with ordinary double-layer latticed domes. Hence, they tend to deflect and oscillate under turbulent wind loadings. As the span increases, the natural frequencies generally decrease and the domes become more vulnerable to resonant excitation. On the other hand, the effective wind load may decrease with an increase in span, due to a size effect related to the spatial correlation of pressure fluctuations. These dynamic changes should be considered appropriately in the structural design of the domes. However, there are many difficult aspects from the viewpoints of aerodynamics and structural mechanics.

---

<sup>†</sup> Associate Professor, Disaster Control Research Center

<sup>‡</sup> Graduate Student, Department of Architecture and Building Science

<sup>††</sup> Professor, New Industry Creation Hatchery Center

<sup>‡‡</sup> Supervisory Research Engineer

Since the wind pressures acting on a dome vary spatially as well as in time, the time-space correlation of the pressure fluctuations may play an important role in the dome's dynamic response. Ogawa *et al.* (1988, 1989) experimentally investigated the time-space correlation of the wind pressures on spherical domes in a wind tunnel and constructed a simple model of the pressure field. Hongo (1995) carried out a series of wind tunnel experiments on the mean and fluctuating wind pressures, in which the focus was on the effects of the turbulence of approaching flow and the dome's geometry on the characteristics of the pressure field. He provided an empirical formula for estimating the design wind loads on the structural frames and members. The size effect is involved in the formula, but the effect of the dome's dynamic response is not considered. Recently, Letchford and Sarkar (2000) published their experimental results on the mean and fluctuating wind pressures acting on smooth and rough parabolic domes. They applied the proper orthogonal decomposition (POD) technique to the fluctuating pressures for analyzing the structure of the pressure field on the dome. It is interesting to note that their results of the POD analysis are in accordance with those of our previous study (Uematsu *et al.* 1997).

Wind-induced dynamic response of domes has been studied by several researchers. For example, Mataka *et al.* (1988) investigated the structural characteristics and wind resistant design of a low-rise cable-reinforced air-supported dome, based on a wind tunnel measurement of wind pressures as well as on a field measurement of the wind-induced response of a large-scale model. Their results indicate that the response can be estimated by applying a quasi-static approach to the estimation of the wind loads. Ogawa *et al.* (1989) made a statistical analysis of the dynamic response for air-supported spherical domes, using the above-mentioned model of the pressure field. Recently, Nakayama *et al.* (1998) proposed a convenient method for evaluating the response of domes through frequency domain analysis, using a limited number of the vibration modes.

The load estimation of the dome's dynamic response has been studied by only a few researchers. Davenport and Surry (1984) measured the steady and fluctuating wind forces on a saddle-shaped hyperboloid (HP) roof and presented a model of the design wind load, represented as an equivalent static load. Their model was based on a peak factor approach and they proposed the values of the dynamic load combination factors  $\gamma$ . However, the basis for determining the values of  $\gamma$  as well as for the mode selection is not clear. Recently, we investigated the design wind load for an elliptic dome, based on the dynamic response analysis both in the time and frequency domains (Uematsu *et al.* 2001b). The results obtained from various approaches were compared with one another. It was found that the peak factor approach gave a reasonable estimation of the design wind load. However, the application of this approach is dependent on how to determine the values of the dynamic load combination factors. An alternative and simpler method is a gust effect factor approach. In our recent study (Uematsu *et al.* 2002a), we have shown that this approach can be applied to the load estimation for circular flat roofs reasonably. Furthermore, the results of our investigation on a single-layer latticed dome imply that the same approach can be applied to such a dome as well (see Uematsu *et al.* 2001a).

This paper discusses the design wind loads for the structural frames of single-layer latticed domes with long spans. The wind pressures are measured simultaneously at many points on dome models in two kinds of turbulent boundary layers, which simulate natural winds over typical open-country and urban terrains. The purpose of the wind tunnel experiment is not to discuss the wind pressures in detail but to obtain wind pressure data to be used for the dynamic response analysis of full-scale domes. For simulating the pressure fluctuations at the nodes of the network, the POD technique is applied to the wind tunnel data. Using the simulated wind pressures, we make two kinds of response analyses. In the first analysis, the dynamic response of several models is analyzed in the

time domain; the nodal displacements and the resultant member stresses (both axial and bending) are computed at each time step. The characteristics of the dynamic response are investigated in detail. It is found that the response is almost quasi-static and the resonant effect on the dynamic response is relatively small. Then, a series of quasi-static analyses, in which the inertia and damping terms are neglected, is made for a wide range of the dome's geometry. Based on the results, we discuss the equivalent pressure coefficient that reproduces the maximum load effects; the focus is on the applicability of the gust effect factor approach. Finally, we provide an empirical formula for the gust effect factor and a simple model of the pressure coefficient distribution. The application of these empirical formulas is investigated by comparing the predicted results by the formulas with those obtained from the quasi-static analysis.

It should be mentioned that this paper is an extended version of our previous papers (Uematsu *et al.* 2001a, 2002b).

## 2. Model domes and their structural properties

The subject of this study is a rigidly jointed single-layer latticed dome with a triangular network. The members are steel pipes ('STK400' as specified in the Japanese Industrial Standard). Table 1 summarizes the dimensions and structural properties of the models, in which  $N_{div}$ ,  $q_{cY}$  and  $S$  represent the division number of the network (see Fig. 1), the buckling load of the dome under

Table 1 Dimensions and structural properties of the dome models

$f/D$	$D$ (m)	$N_{div}$	$d$ (mm) $\times$ $t$ (mm)	$q_{cY}$ (kN/m <sup>2</sup> )	$S$	$f_1$ (Hz)
0.05	120	8	812.8 $\times$ 19.0	16.48	0.77	1.75
(Low-rise)	180	10	1117.6 $\times$ 28.0	16.95	1.09	1.52
0.10	120	8	500.0 $\times$ 14.0	16.84	1.40	1.90
(Middle-rise)	180	10	660.4 $\times$ 22.0	16.92	1.36	1.66
0.20	120	8	355.6 $\times$ 9.0	16.47	2.38	2.07
(High-rise)	180	10	508.0 $\times$ 12.0	16.65	1.77	1.75

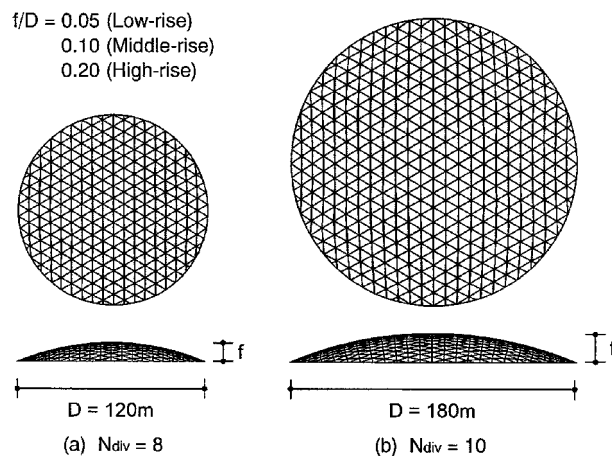


Fig. 1 Network of the dome

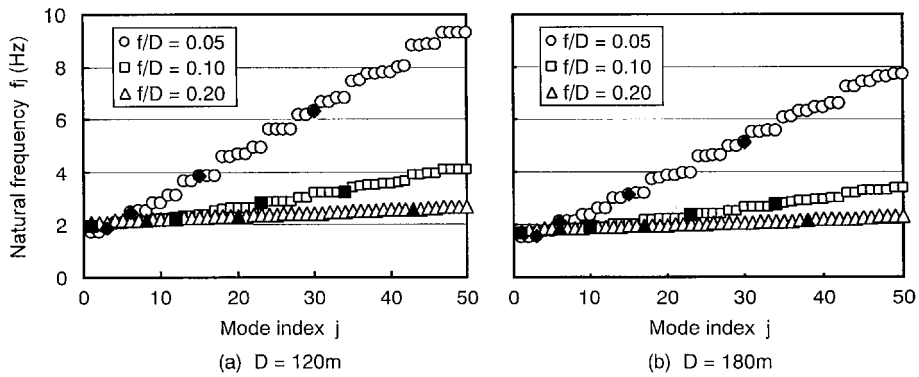


Fig. 2 Natural frequencies of the dome

uniform pressure and the shell likeness factor, respectively. The definition of these parameters is given in Yamada (1984) and in Yamada and Ishikawa (1987). The rise/span ratios ( $f/D$ ) are 0.05, 0.10 and 0.20; in this paper, they are referred to as ‘low-rise’, ‘middle-rise’ and ‘high-rise’, respectively. The members arranged on the boundary are assumed to be clamped on a circular rigid wall; the results of a preliminary analysis indicated that the fundamental characteristics of the wind-induced response were not affected by the boundary condition significantly. The dome’s dead load  $W_d$  and the design snow load  $W_s$  per unit area are assumed 1.98 and 0.49 kN/m<sup>2</sup>, respectively, as representative values. The dimensions (outer diameter  $d \times$  thickness  $t$ ) of the members are determined so that the value of  $q_{cY}$  becomes approximately six times as large as  $(W_d + W_s)$ ; a description of the buckling analysis of latticed domes is presented in Yamada (1984). This criterion

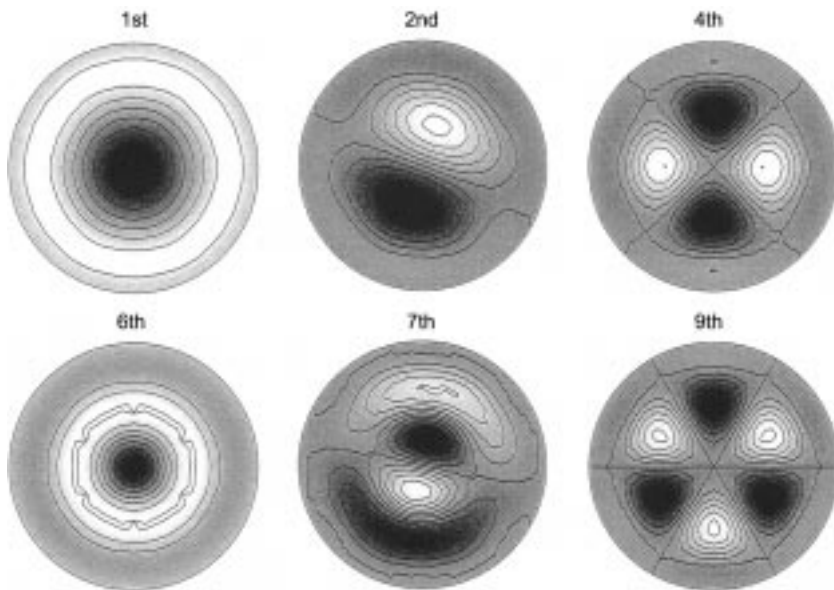


Fig. 3 Mode shapes of vibration ( $D=180\text{ m}$ ,  $f/D=0.20$ )

is often used for designing long-span domes in Japan.

The natural frequencies  $f_j$ , up to the 50th mode ( $j=1-50$ ), are plotted in Fig. 2; the closed symbols correspond to the axisymmetric modes of vibration. Sample results for the mode shapes  $\{\phi\}_j$  of vibration are schematically illustrated in Fig. 3. In the case of this model, the 1st and 6th modes are regarded as axisymmetric. Each asymmetric mode has its counterpart with the same natural frequency and a vibration mode that is the same in shape but rotated about the axis of revolution. For example, regarding the 2nd and 3rd modes, the natural frequencies are the same and the corresponding vibration modes are perpendicular to each other. Fig. 2 indicates that the natural frequencies are fairly close to one another, particularly for the high-rise dome ( $f/D=0.20$ ). This is one of the most important considerations when analyzing the dynamic response and estimating the design wind loads of single-layer latticed domes.

### 3. Wind tunnel measurements and reconstruction of pressure field

#### 3.1. Experimental arrangements and procedures

The experiments were carried out in a closed-circuit-type wind tunnel at Kajima Technical Research Institute, which has a working section 18.1 m long, 2.5 m wide and 2.0 m high. Two kinds of turbulent boundary layers, which simulated the natural winds over typical open-country and urban terrains, were generated with a standard spire-roughness arrangement on the wind tunnel floor; in this paper, these flows are referred to as Flows 'I' and 'II', respectively. The power law exponent of the mean velocity profile is approximately 0.15 for Flow I and 0.27 for Flow II. The geometric scale of these flows ranges from 1/400 to 1/500.

The geometry of the wind tunnel model is schematically illustrated in Fig. 4(a). The eaves-height/span ratio ( $h/D$ ) is varied from 0 to 1 with a step of 1/16. The span  $D$  of the wind tunnel models is 267 mm. Hence, the geometric scale  $\lambda_L$  of the wind tunnel models is 1/449 for  $D=120$  m and 1/674 for  $D=180$  m. There is a slight mismatch in the geometric scale between the wind tunnel model and flow. However, it is thought that the effect of this discrepancy on the wind pressures is not significant (see Davenport *et al.* 1977, for example). Therefore, the wind tunnel data can be used for the dynamic response analyses of the full-scale domes with consideration of the similarity law. The surface of the model is nominally smooth. Each model is equipped with 433 pressure taps of 0.5 mm diameter, as shown in Fig. 4(b). The pressure taps are connected to pressure transducers (Zoc, 13B/8Px MUXLESS) in parallel via 80 cm lengths of flexible vinyl tubing of 1 mm inside diameter. The compensation for the frequency response of this pneumatic tubing system is carried out by using a digital filter, which is designed so that the dynamic data up to approximately 500 Hz can be obtained without distortion. The signals from the transducers are sampled in parallel at a rate of 1 kHz on each channel for a period of approximately 33 s. All measurements are made at a wind velocity of  $U_{ref}=10$  m/s at a reference height of  $Z_{ref}=267$  mm. The wind velocity  $U_{top}$  at the level of rooftop ranges from approximately 5.3 to 10.2 m/s; the corresponding Reynolds number  $Re$ , defined in terms of  $D$  and  $U_{top}$ , ranges from approximately  $9.4 \times 10^4$  to  $1.8 \times 10^5$ . The turbulence intensity  $I_{u,top}$  at the level of rooftop ranges from 0.13 to 0.20 for Flow I and from 0.12 to 0.27 for Flow II. The wind-tunnel blockage ratio is less than 2% in any case. For such small values, the blockage effect on the wind pressures is considered insignificant. Therefore, no correction is applied to the results. The details of the experimental arrangements and procedures are given in Hongo (1995) and Uematsu *et al.* (1997).

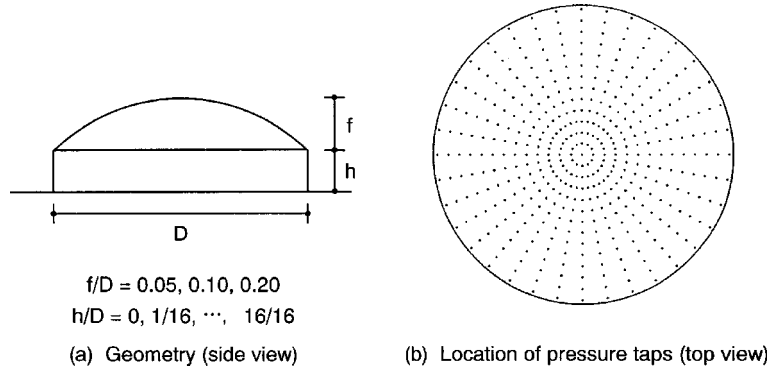


Fig. 4 Wind tunnel model

### 3.2. Reconstruction of pressure field by using POD technique

Since the location of the nodes of the dome's network does not coincide with that of the pressure taps (compare Figs. 1 and 4(b) with each other), we cannot use the wind-tunnel pressure data directly in the dynamic response analysis of the full-scale domes. Therefore, it is necessary to simulate the pressure fluctuations at the nodes. For this purpose, we apply the POD technique to the wind-tunnel pressure data; in the application, we consider the non-uniform distribution of pressure taps (regarding the details of this technique, see Taniguchi *et al.* 1996 and Jeong *et al.* 2000, for example).

The POD analysis calculates the eigenvalue  $\lambda_k$  and corresponding eigenvectors  $\{\Phi\}_k$  ( $k=1-433$ ) from the covariance matrix of the fluctuating pressures. The pressure field  $\{p(t)\}$  may be represented by the following equation :

$$\{p(t)\} = q_{ref}\{C_p(t)\} = q_{ref}\sum_{k=1}^N a_k(t)\{\Phi\}_k \quad (1)$$

where  $q_{ref}$ =reference velocity pressure, which defines the pressure coefficient  $C_p(t)$ ;  $N$ =number of terms used for the simulation; and  $a_k(t)$  represents the expansion coefficient. The velocity pressure  $q_{ref}$  is defined by the wind velocity  $U_{top}$  at the level of rooftop or by the wind velocity  $U_H$  at the mean roof height  $H$ . The eigenvalue  $\lambda_k$  is the measure of the contribution of each eigenvector to the pressure mean squares. It is normalized as follows :

$$P_k = \frac{\lambda_k}{\sum_{j=1}^{433} \lambda_j} \quad (2)$$

Sample results on the normalized eigenvalues are shown in Fig. 5. The first eigenvector generally contributes to the pressure mean squares by 40–50%. The accumulated values of  $P_k$  up to the 8th and up to the 25th eigenmode are approximately 0.8 and 0.9, respectively. In the following analysis, we simulate the wind pressures at the nodes of the dome's network using the first 25 eigenvectors ( $N=25$  in Eq. (1)). The values of  $\{\Phi\}_k$  ( $k=1-25$ ) at the nodes are interpolated or extrapolated from

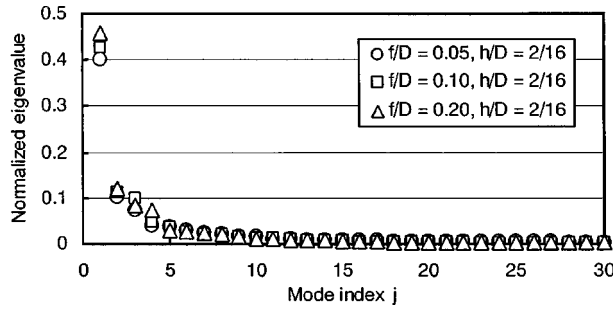


Fig. 5 Normalized eigenvalues of pressure ( $h/D=2/16$ , Flow II)

those at the pressure taps using MATLAB (a bicubic function). With these 25 eigenvectors, we cannot simulate the pressure fluctuations of higher frequencies. However, such high-frequency fluctuations may not contribute to the general response of the dome significantly, because the spatial correlation of such fluctuations is rather low (see Hongo 1995) and, furthermore, their frequencies are much higher than the dome's natural frequencies under consideration.

#### 4. Dynamic response analysis for selected dome models

##### 4.1. Method of analysis

In this section, eight models are used for analysis. The geometry of the models is as follows :

$$D=120 \text{ m}, 180 \text{ m}; \quad f/D=0.10, 0.20; \quad h/D=2/16, 4/16$$

In our previous study (Uematsu *et al.* 1994), we found that the dome's static deformation due to the time-averaged wind pressure did not affect the natural frequencies and vibration modes significantly up to an ordinary design wind velocity, such as  $U_{top}=40-50$  m/s, for example. Therefore, the dynamic motion of the dome can be represented by a linear system. Applying a finite element method to the latticed dome, we obtain the following equation of motion for the nodal displacements  $\{u(t)\}$  (regarding the details of this equation, see Liu *et al.* 1996) :

$$[M]\{\ddot{u}(t)\} + [C]\{\dot{u}(t)\} + [K]\{u(t)\} = \{P(t)\} \quad (3)$$

where  $[M]$ ,  $[C]$ ,  $[K]$  are mass, damping and stiffness matrices, respectively; and  $\{P(t)\}$  represents the wind load vector, which consists of the nodal loads. We assume that the damping matrix is given by the following equation (Rayleigh damping) :

$$[C]=a_M[M]+a_K[K] \quad (4)$$

For determining the values of  $a_M$  and  $a_K$ , the critical damping ratios of the first and second modes are assumed 0.02, which is often used in the design of steel structures. The effects of aerodynamic damping and stiffness on  $[C]$  and  $[K]$  are not considered. Such an assumption may result in an

Table 2 Similarity law of the wind tunnel experiment for the dynamic analysis

$D$ (m)	$\lambda_L$	$h/D$	$\lambda_V$		$\lambda_T$	
			Flow I	Flow II	Flow I	Flow II
120	1/449	2/16	1/6.8	1/8.4	1/66	1/53
		4/16	1/6.4	1/7.5	1/60	1/60
180	1/674	2/16	1/6.8	1/8.4	1/99	1/80
		4/16	1/6.4	1/7.5	1/105	1/90

overestimation or underestimation of the response to some degree. However, the effects have not been clarified yet in a quantitative sense; this is the subject of a future study. Furthermore, the effect of internal pressure is not considered either; this subject is beyond the scope of this study. Hereafter, we deal with only the wind-induced response, i.e. the increment or decrement from the equilibrium state of the dome subjected to the deal load in still air.

Eq. (3) is numerically integrated by using the Newmark  $\beta$  method with  $\beta=1/4$ . The time step  $\Delta t$  for the numerical integration is 1/500 s, which is smaller than 1/200 of the first natural period  $T_1 (=1/f_1)$  of the dome. The wind load  $P(t)$ , expressed as a concentrated load at the node of the network, is given by the product of the wind pressure  $p(t)$  at the location of the node and the tributary area of the node. The wind velocity  $U_h$  at the eaves-height  $h$  is assumed 50 m/s. The velocity scale  $\lambda_V$  and the corresponding time scale  $\lambda_T$  of the wind tunnel experiment are summarized in Table 2. The time step (sampling interval)  $\Delta t_p$  of the pressure measurements in the wind tunnel experiment corresponds to  $\sim 0.1$  s in full scale. Since the value of  $\Delta t_p$  is much longer than  $\Delta t$ , we apply the Spline functions of the third order to the discrete values of  $a_k(t)$  in Eq. (1) for obtaining the intermediate values of the pressure coefficient  $C_p(t)$ . The solution of Eq. (3) is expressed as a time history of the displacement vector  $\{u(t)\}$ . Hence, in order to investigate the dynamic response in each vibration mode, the modal displacements  $A_j(t)$  ( $j=1-150$ ) are also computed by the following equation :

$$A_j(t) = \{\phi\}_j^T \{u(t)\} \quad (5)$$

Furthermore, the resultant member stresses (both axial and bending) are also computed at each time step.

The dome's response is analyzed for a time duration of 11 min in total for each run. The result for the first 1 min is not used for the statistical analysis of the response because of the non-stationarity. The number of runs ranges from 3 to 5, depending on the time scale determined from the geometric and velocity scales of the wind tunnel experiment. The results presented here are all the expected values obtained by applying ensemble averaging to the results of these runs. In addition to the statistical properties of the responses, we focus on the deflection and the resultant member stresses at the instant when the response, i.e., the deflection at a node or the stress involved in a member, becomes the maximum during a time duration of 10 min.

#### 4.2. Characteristics of the dynamic response of domes

Fig. 6 shows the distribution of the axial stresses involved in the members at the instant when each

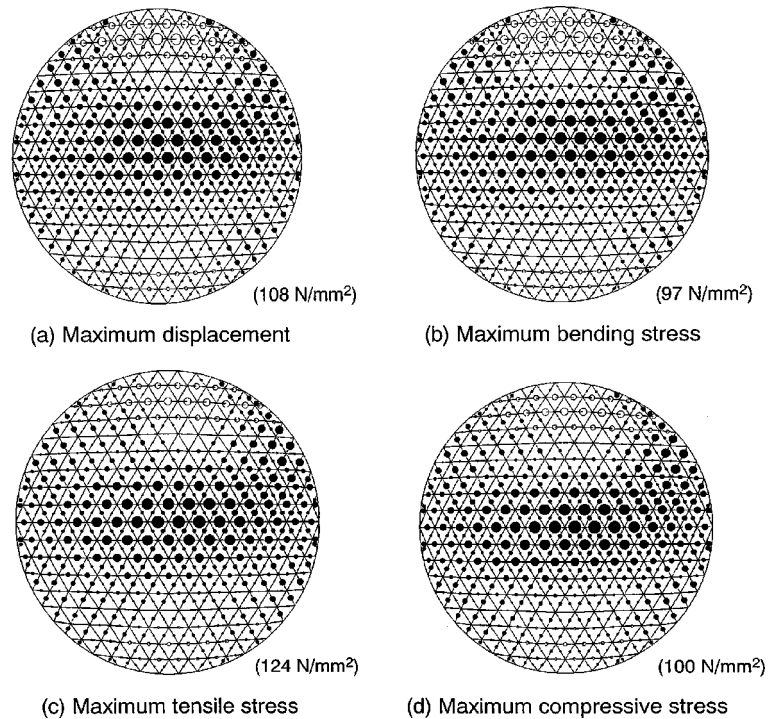


Fig. 6 Distribution of the axial stresses involved in the members at the instant  $t_0$  when each of the four responses (deflection, bending, tensile and compressive stresses) becomes the maximum ( $D=120$  m,  $f/D=0.2$ ,  $h/D=2/16$ , Flow II)

response becomes the maximum for a high-rise dome ( $f/D=0.2$ ), in which the deflection, the axial (both tensile and compressive) and bending stresses are considered as the responses, or the load effects. The diameter of each circle is proportional to the magnitude of the stress involved in each member. The open and closed circles represent the compressive and tensile stresses, respectively. The value in the parentheses represents the maximum stress among all members. It is found that the stress distributions are similar to one another both in pattern and in magnitude.

Shown in Fig. 7 are the values of the modal displacements at the instant  $t_0$  when each of the four responses becomes the maximum. For example, the circles represent the modal displacements at the instant when the maximum displacement occurs at a node during a time duration of 10 min. The value of  $A_j(t_0)$  is regarded as an indicator of the contribution of the  $j$ -th mode to the maximum response. In the high-rise dome case (Fig. 7(b)), the values of  $A_j(t_0)$  for the four responses are almost the same, particularly for the first mode. Therefore, it is thought that the four maximum responses are induced almost simultaneously. This feature corresponds well to the above-mentioned fact that we observed similar stress distributions for the four maximum responses in Fig. 6. In the middle-rise dome case (Fig. 7(a)), on the other hand, the values of  $A_j(t_0)$  for the four responses are different from one another. This feature indicates that the four maximum responses occur at different times. The values of  $A_j(t_0)$  in Fig. 7 include both the time-averaged (static) and the dynamic components. Then, the results for the static and dynamic components are plotted separately in Figs. 8 and 9, respectively. The closed symbols in Fig. 8 correspond to the axisymmetric modes of vibration. It is

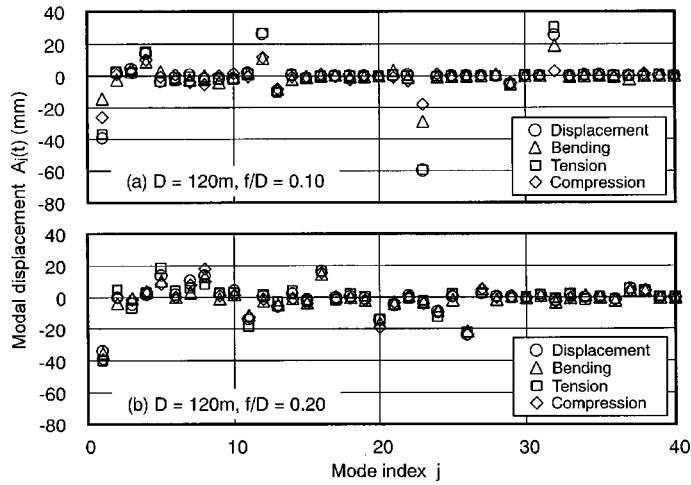


Fig. 7 Characteristics of the modal displacement  $A_j(t_0)$  ( $h/D=2/16$ , Flow II)

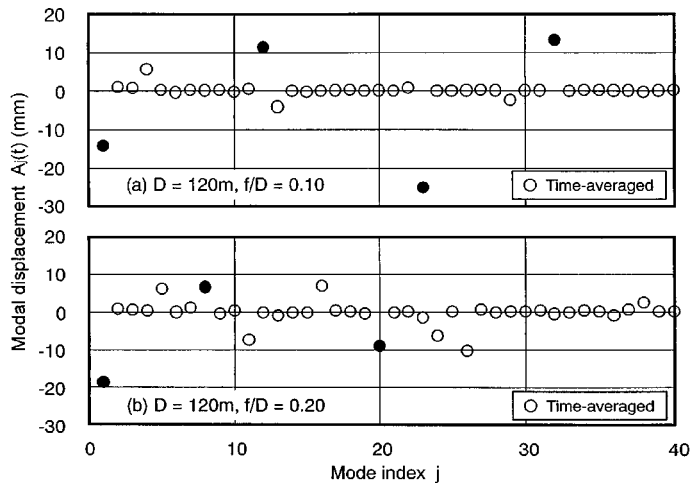


Fig. 8 Characteristics of the static component of the modal displacement  $A_j(t_0)$  ( $h/D=2/16$ , Flow II)

found that the general response, including the static component, is dominated by several lower asymmetric modes (such as  $j < 10$ , for example) as well as by the first three to four axisymmetric modes. Most of these modes contribute to the static components as well (compare Figs. 7 and 8 with each other). In other words, the dome's general response is dominated by such modes that contribute to the static response significantly. From these results, it is thought that the dynamic response of the domes under consideration is almost quasi-static; that is, the effect of resonance on the dynamic response is relatively small.

Based on the above-mentioned discussion, we made a series of quasi-static analyses as the next step. "Quasi-static response" refers to the response that follows the fluctuating gust forces below the natural frequencies of the dome under consideration and it can be computed by solving the

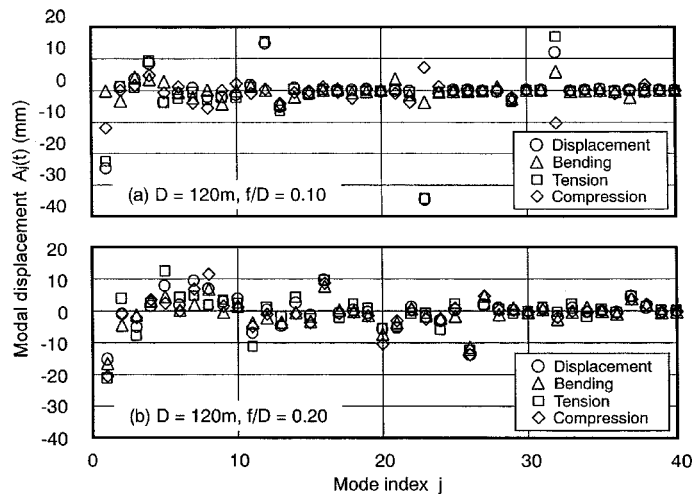


Fig. 9 Characteristics of the dynamic component of the modal displacement  $A_j(t_0)$  ( $h/D=2/16$ , Flow II)

Table 3 Comparison for the maximum member stress (unit:  $N/mm^2$ ) between the dynamic and quasi-static analyses ( $D=120$  m)

$f/D$	$h/D$	Flow	Dynamic analysis		Quasi-static analysis	
			Axial stress	Bending stress	Axial stress	Bending stress
0.10 (Middle-rise)	2/16	I	41.4	48.1	38.9	46.0
	4/16	I	42.7	96.9	39.1	90.6
	2/16	II	59.6	88.5	52.0	85.5
	4/16	II	53.9	151	46.5	132
0.20 (High-rise)	2/16	I	104	132	93.0	121
	4/16	I	97.2	103	93.2	96.3
	2/16	II	125	174	121	165
	4/16	II	116	150	117	150

equation of motion in which the inertia and damping terms are neglected. Table 3 shows a comparison for the maximum member stresses (axial and bending) between the dynamic analysis and the quasi-static analysis for the  $D=120$  m domes; similar results were obtained for the  $D=180$  m domes. It can be seen that the difference between these two analyses is relatively small, up to about 10 percents at the most. This result confirms the above-mentioned inference that the dome's response is almost quasi-static. Such a feature may lead to a simple procedure for estimating the design wind loads, as will be described in the following section.

## 5. Estimation of design wind load based on quasi-static analysis

### 5.1. Basic concept and assumptions

In this section, we discuss the design wind loads for the structural frames of the domes, based on a series of quasi-static analysis for a wide range of the dome's geometry as follows :

$$D=120, 180 \text{ m}; \quad f/D=0.05, 0.10, 0.20; \quad h/D=0, 1/16, 2/16, \dots, 16/16$$

The number of the dome models analyzed here is 102. Because an emphasis is on the systematic analysis, some of the models seem unrealistic. The wind velocity  $U_H$  at the mean roof height  $H$  is given by the following equation, according to the AIJ Recommendations for Loads on Buildings (1993) :

$$U_H = U_0 \times 1.7 \left( \frac{H}{Z_G} \right)^\alpha \quad (6)$$

where  $U_0$  represents the 'basic wind velocity', i.e., 10-min mean wind velocity with a 100-yr mean recurrence interval at a height of 10 m above ground for flat and open exposure;  $Z_G$  is a representative height, roughly corresponding to the gradient height of the atmospheric boundary layer; and  $\alpha$  is the power law exponent of the mean velocity profile. The basic wind velocity  $U_0$  is assumed 35 m/s, which covers most of the Main Island of Japan. The values of  $\alpha$  and  $Z_G$  are respectively 0.15 and 350 m for Flow I (open-country terrain) and 0.27 and 550 m for Flow II (urban terrain). The velocity scale  $\lambda_v$  and the corresponding time scale  $\lambda_T$  of the wind tunnel experiment are summarized in Table 4. Note that the values of  $\lambda_v$  and  $\lambda_T$  are different from those used in Section 4.2. If the mean velocity profile of the wind tunnel flow is perfectly similar to that represented by Eq. (6), the values of  $\lambda_v$  and  $\lambda_T$  become independent of  $H$ . In practice, however, they are somewhat dependent on the model configuration.

### 5.2. Application of gust effect factor approach

Fig. 10 shows sample results on the relation between the maximum stress  $\sigma_{\max}$  during a time duration of 10 min and the time-averaged stress  $\bar{\sigma}$  for all members. Regarding the axial stress, the absolute values are used both for the tensile and compressive stresses. It is found that the data

Table 4 Similarity law of the wind tunnel experiment for the quasi-static analysis

$D$ (m)	$f/D$	$\lambda_L$	$\lambda_v$		$\lambda_T$	
			Flow I	Flow II	Flow I	Flow II
120	0.05	1/449	1/4.9–1/5.2	1/3.3–1/4.2	1/91–1/86	1/134–1/106
	0.10	1/449	1/5.0–1/5.3	1/3.7–1/4.2	1/90–1/86	1/122–1/106
	0.20	1/449	1/5.0–1/5.3	1/4.0–1/4.2	1/89–1/85	1/114–1/107
180	0.05	1/674	1/5.2–1/5.5	1/3.7–1/4.7	1/129–1/122	1/182–1/143
	0.10	1/674	1/5.3–1/5.6	1/4.1–1/4.7	1/127–1/121	1/164–1/142
	0.20	1/674	1/5.4–1/5.6	1/4.4–1/4.7	1/127–1/120	1/153–1/144

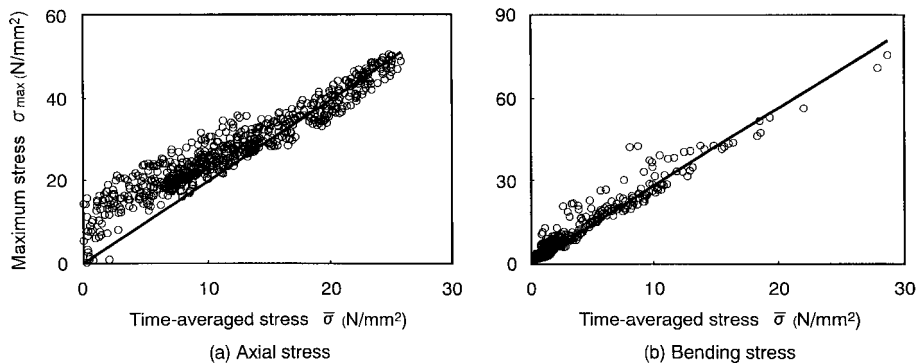


Fig. 10 Relation between  $\sigma_{\max}$  and  $\bar{\sigma}$  ( $D=120$  m,  $f/D=0.20$ ,  $h/D=2/16$ , Flow I)

collapse into a relatively narrow region around the regression line represented by a thick solid line. The regression line was obtained by fitting it to the largest 10 percent of the data for  $\sigma_{\max}$ . The slope of this line approximately corresponds to the gust effect factor  $G_f$ . Therefore, the results indicate that the gust effect factor approach can be used for estimating the design wind loads; that is, the design wind load may be represented as an equivalent static load, given by the product of the time-averaged wind load and the gust effect factor  $G_f$ . Although there exists a large scatter in the data for smaller  $\bar{\sigma}$  values in some cases, this is not a serious problem in practice, because the size of the members is generally determined based on the maximum stress among all members.

Regarding the values of  $G_f$ , the following features were observed :

- (1) The value for the bending stress is larger than that for the axial stress.
- (2) The value in Flow II is larger than that in Flow I. This is due to higher turbulence intensity of the approaching flow.
- (3) The value for  $D=180$  m is smaller than that for  $D=120$  m. This is due to a size effect related to the space correlation of pressure fluctuations on the dome.
- (4) The value for the middle-rise dome is larger than that for the low-rise and high-rise domes. This may be due to a complicated change of the pressure field with the rise/span ratio.

According to the common procedure used for structural design, we focus on the extreme fiber stress  $\sigma_{fb}$  involved in the cross section of the member, as the most important load effect for the single-layer latticed domes. The extreme fiber stress is induced by the axial force and bending moment; that is, tensile stress plus bending stress (positive) or compressive stress minus bending stress (negative). In the following, we consider the values of  $\sigma_{fb}(t_0)$  at the instant  $t_0$  when the maximum value of  $\sigma_{fb}$  occurs during a time duration of 10 min, as we did in the previous section.

Fig. 11 shows the relation between the value of  $\sigma_{fb}(t_0)$  and the time-averaged value  $\bar{\sigma}_{fb}$  for all members. In the figure,  $\sigma_{fb}(t_0)$  and  $\bar{\sigma}_{fb}$  are both reduced by the yield stress  $\sigma_Y$  of the members (assumed  $235$  N/mm<sup>2</sup>). As might be expected from the above-mentioned results, an approximately linear relation between these two values can be seen. The same results are represented in a different manner in Fig. 12; that is, the data are plotted in order of increasing values of  $\sigma_{fb}(t_0)$  and  $\bar{\sigma}_{fb}$ . When plotted in such a manner, the values of  $\sigma_{fb}(t_0)$  and  $\bar{\sigma}_{fb}$  represented by a circle in the figure do not correspond to the same member. The scatter of the data decreases considerably, compared with that in Fig. 11. The slope of a straight line connecting the origin to the point of the largest  $\sigma_{fb}(t_0)$  value, not shown in the figure, stands for an equivalent gust effect factor, which predicts the

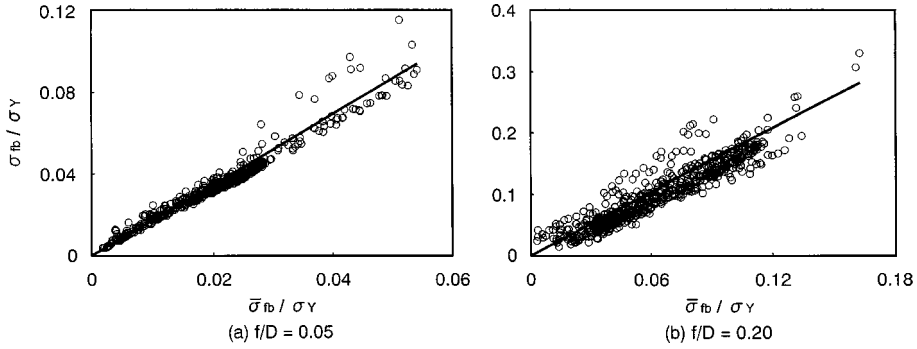


Fig. 11 Relation between  $\sigma_{fb}(t_0)$  and  $\bar{\sigma}_{fb}$  ( $D=120$  m,  $h/D=2/16$ , Flow I)

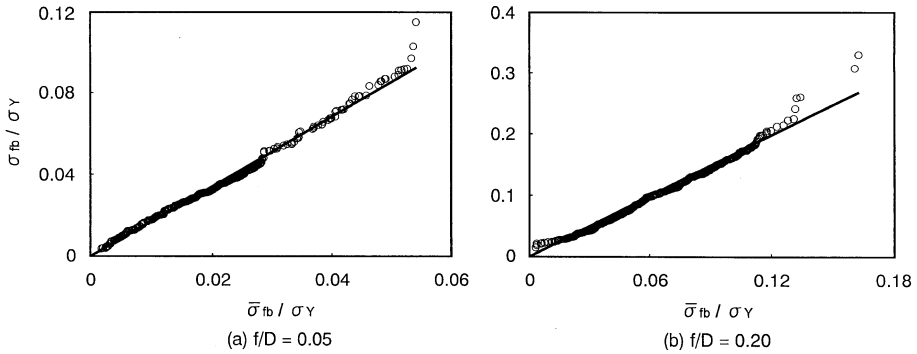


Fig. 12 Relation between  $\sigma_{fb}(t_0)$  and  $\bar{\sigma}_{fb}$ , plotted in order of increasing values ( $D=120$  m,  $h/D=2/16$ , Flow I)

maximum peak stress among all members, when used together with the time-averaged loads. Such a definition of the gust effect factor is not correct in the strict sense. However, considering that single-layer latticed domes usually consist of members of the same cross section and the dimension of the members is determined based on the maximum peak stress, the load estimation by using such an equivalent gust effect factor  $G_f$  may be reasonable from the practical viewpoint.

### 5.3. Empirical formula for gust effect factor

The values of  $G_f$  obtained from the above-mentioned procedure for  $f/D=0.05$  and  $0.20$  are plotted against  $h/D$  in Fig. 13. When rearranging the data for various cases, we found that the variation of  $G_f$  with the turbulence intensity  $I_{uH}$  of the approaching flow at the mean roof height  $H$  and with the  $H/D$  ratio was similar to that for circular flat roofs. In our previous paper (Uematsu *et al.* 2002a), we provided an empirical formula for the gust effect factor  $G_{f,flat}$  of circular flat roofs as follows :

$$G_{f,flat} = 1 + g \cdot r_F \cdot R \tag{7}$$

$$g \approx \sqrt{2 \ln 600 f_1} + \frac{0.577}{\sqrt{2 \ln 600 f_1}} \tag{8}$$

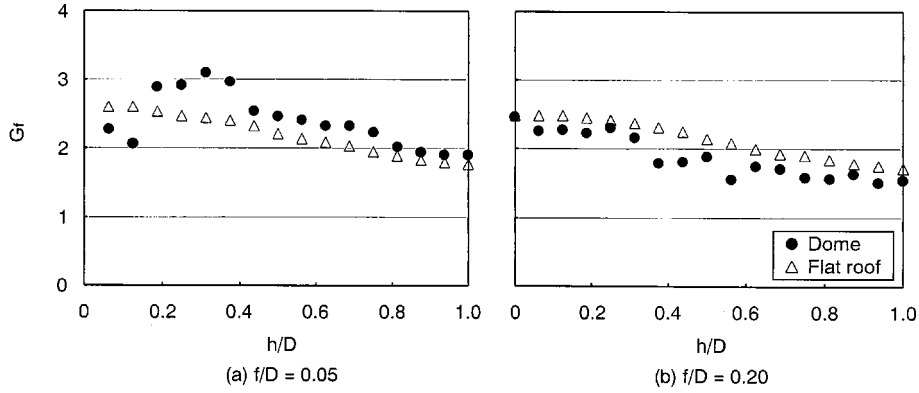


Fig. 13 Gust effect factors for single-layer latticed domes and circular flat roofs ( $D=120$  m, Flow II)

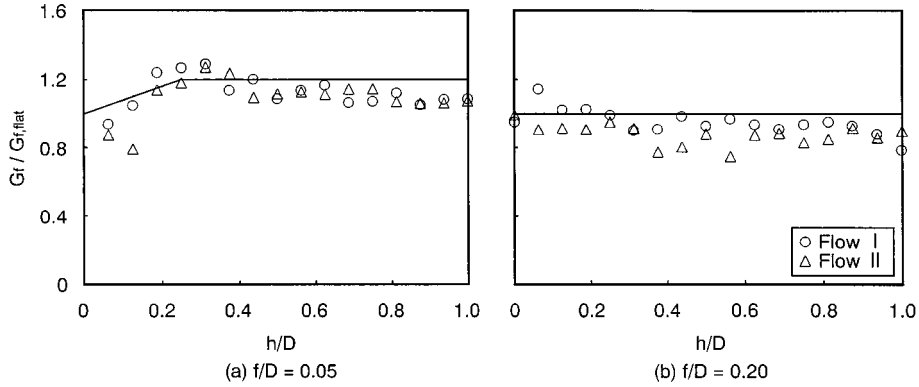


Fig. 14 Ratio of the gust effect factor  $G_f$  to the corresponding flat-roof value  $G_{f,flat}$  ( $D=120$  m, Flows I and II)

$$r_F = 3.4I_{uH}^2 \cdot \exp\left(0.04\frac{D}{H}\right) + 0.12 \quad (9)$$

where  $g$ =peak factor;  $r_F$ =ratio of the rms to the mean modal force coefficient of the first axisymmetric mode;  $R$ =resonant magnification factor; and  $f_1$ =natural frequency of the first axisymmetric mode. When  $D/H > 7$ , we may substitute 7 for  $D/H$  in Eq. (9). Because we deal with the quasi-static response in this section,  $R$  is regarded as 1.0. Furthermore, we may assume that  $g=4.0$  for the purpose of simplicity. The values of  $G_{f,flat}$  predicted by the formula are also plotted in Fig. 13. The results imply that we can estimate the gust effect factor  $G_f$  for the single-layer latticed domes by using the formula for  $G_{f,flat}$ , although some modification of the formula should be made. Figs. 14(a) and 14(b) show the ratio of  $G_f$  to  $G_{f,flat}$  for  $f/D=0.05$  and  $0.20$ , respectively. It was found that the variation of the  $G_f/G_{f,flat}$  ratio with  $h/D$  can be approximated by the following equations (a line graph in Fig. 14) :

$$\frac{G_f}{G_{f,flat}} = \begin{cases} 4(C_{\max} - 1)\frac{h}{D} + 1.0 & \left(\text{for } 0 \leq \frac{h}{D} \leq 0.25\right) \\ C_{\max} & \left(\text{for } 0.25 < \frac{h}{D} \leq 1.0\right) \end{cases} \quad (10)$$

$$C_{\max} = \begin{cases} 1.0 + 4\frac{f}{D} & \left(\text{for } 0 \leq \frac{h}{D} \leq 0.1\right) \\ 1.8 - 4\frac{f}{D} & \left(\text{for } 0.1 < \frac{h}{D} \leq 0.2\right) \end{cases} \quad (11)$$

Using Eqs. (7)–(11), we can easily estimate the gust effect factor  $G_f$  for single-layer latticed domes with  $f/D=0-0.2$  and  $h/D=0-1.0$ .

#### 5.4. Equivalent pressure coefficient

A discussion is made of the equivalent pressure coefficients, which reproduce the same load effects that the practical pressure distribution induces. Fig. 15 shows a model of the pressure coefficient distribution on the dome. The dome is divided into four regions, labeled as ‘R1’ to ‘R4’, and the pressure coefficient in each region is assumed constant. The value of the equivalent pressure coefficient in each region is given by spatially averaging the pressure coefficient distribution over the region. The results of the equivalent pressure coefficients  $C_{p1}$  to  $C_{p4}$  for the four regions are plotted against  $h/D$  in Fig. 16. It was found that the values were not affected by the turbulence intensity of the approaching flow significantly. They depend on  $f/D$  as well as on  $h/D$ . The variation of  $C_{pi}$  ( $i=1-4$ ) with  $h/D$  for a constant  $f/D$  ratio can be represented by a line graph, as shown in Fig. 16. The values of  $C_{pi}$  ( $i=1-4$ ) for  $h/D=0, 0.25$  and  $1.0$  are summarized in Table 5. These values were determined not only from the present results but also from the results of the previous

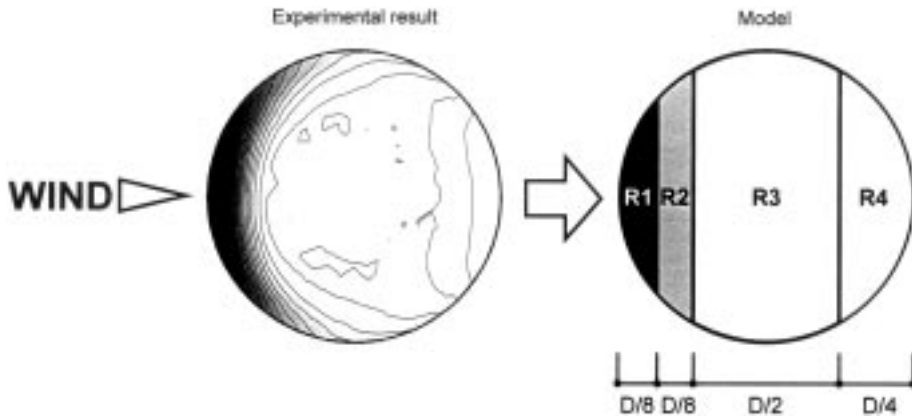


Fig. 15 Model of pressure coefficient distribution on the dome

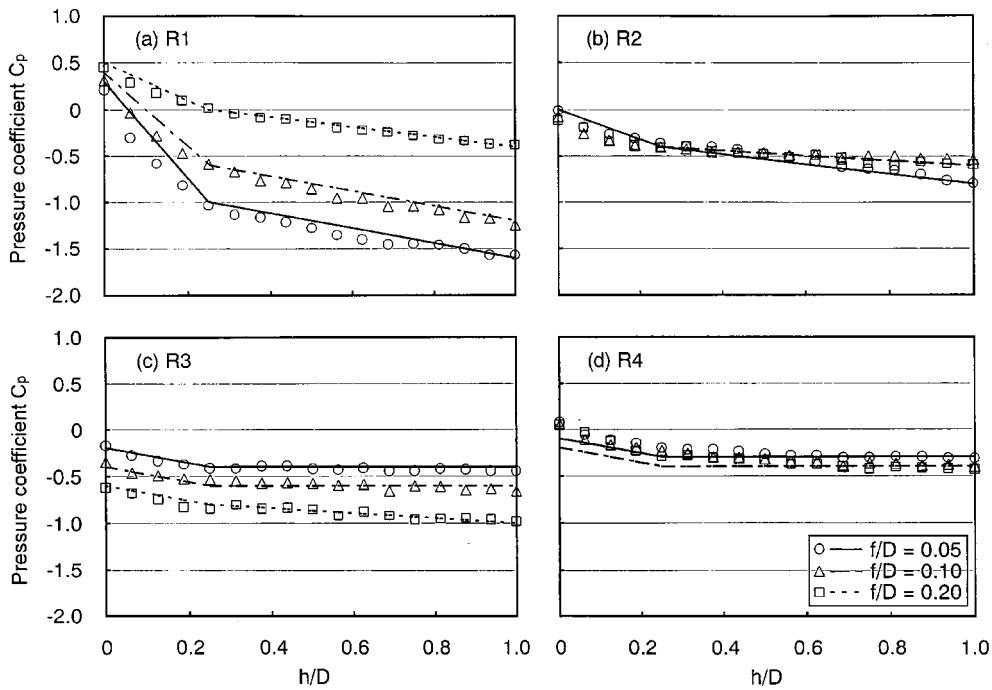


Fig. 16 Equivalent pressure coefficients  $C_{p1}$  to  $C_{p4}$  for the four regions R1 to R4 (Flow I)

Table 5 Equivalent pressure coefficient  $C_{pi}$  ( $i=1-4$ ) in each region for  $h/D=0, 0.25$  and  $1.0$

$f/D$	$h/D=0$				$h/D=0.25$				$h/D=1.0$			
	R1	R2	R3	R4	R1	R2	R3	R4	R1	R2	R3	R4
0.05	0.3	0.0	-0.2	-0.1	-1.0	-0.4	-0.4	-0.3	-1.6	-0.8	-0.4	-0.3
0.10	0.4	0.0	-0.4	-0.2	-0.6	-0.4	-0.6	-0.4	-1.2	-0.6	-0.6	-0.4
0.20	0.5	0.0	-0.6	-0.2	0.0	-0.4	-0.8	-0.4	-0.4	-0.6	-1.0	-0.4

investigations (for example, Ogawa *et al.* 1988, Suzuki *et al.* 1987, and Fukushi *et al.* 1991).

### 5.5. Validity of the models of gust effect factor and pressure coefficient distribution

First, in order to investigate the validity of the model of the pressure coefficient distribution (Figs. 15 and 16), the maximum value of  $\bar{\sigma}_{fb}$  among all members predicted by the model was compared with that by the practical pressure distribution. Figs. 17(a) and 17(b) show the results for  $f/D=0.05$  and  $0.20$ , respectively. It is found that the agreement is generally good.

Then, a similar comparison was made for the maximum peak stress among all members between the prediction by using the models of  $G_f$  and  $C_p$ -distribution and that obtained from the quasi-static analysis. The results for  $f/D=0.05$  and  $0.20$  are shown in Figs. 18(a) and 18(b), respectively. Again, a relatively good agreement can be seen. Fig. 19 shows histograms of the ratio of the predicted value to that from the quasi-static analysis for the maximum peak stress; the number of data is 204.

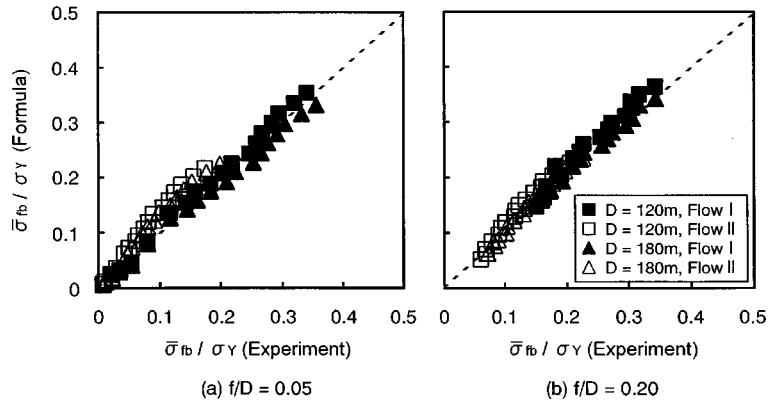


Fig. 17 Comparison of the maximum value of  $\bar{\sigma}_{fb}$  predicted by the pressure distribution model with those computed by using the practical pressure distribution (Flows I and II)

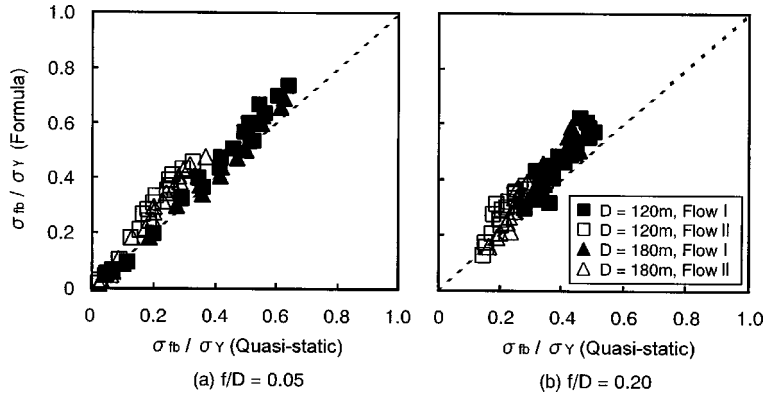


Fig. 18 Comparison of the maximum extreme fiber stress predicted by the  $G_f$  and  $C_p$ -distribution models with that obtained from the quasi-static analysis (Flows I and II)

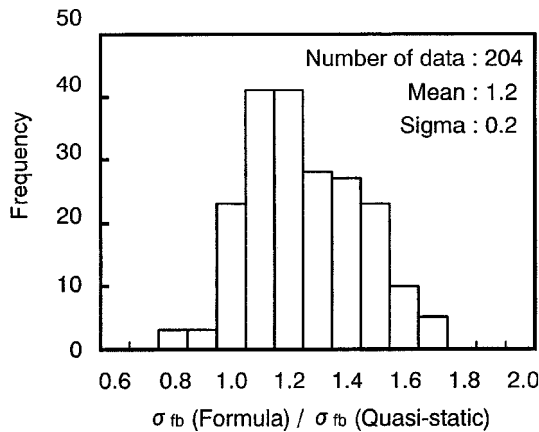


Fig. 19 Ratio of the maximum extreme fiber stress predicted by the formulas to that obtained from the quasi-static analysis

The mean and the coefficient of variance of the data are 1.2 and 0.17, respectively. The formulas present somewhat conservative prediction for the maximum load effects. However, it is concluded that they can be used for estimating the design wind loads with an allowable error, despite the simple model.

## 6. Conclusions

The wind-induced dynamic response and the resultant load estimation of rigidly jointed single-layer latticed domes with long spans have been investigated, based on a series of dynamic response analyses in the time domain. The dome models are designed based on a criterion often used in the structural design of long span domes. The main findings are summarized as follows :

- (1) The dynamic response of the dome is generally dominated by such vibration modes that contribute to the static response significantly, i.e., a few lower axisymmetric and asymmetric modes. In particular, the contribution of the first axisymmetric mode is great.
- (2) The dome's response is almost quasi-static. In other words, the effect of resonance on the dynamic response is relatively small. Therefore, the dynamic response can be evaluated by the quasi-static analysis, in which the inertia and damping terms are neglected.
- (3) The design wind load can be estimated by the gust effect factor approach. At least, this approach captures the maximum member stresses with an allowable error.
- (4) In this study, the focus is on the extreme fiber stress involved in the cross section of the member, as the most important load effect. The gust effect factor, defined in terms of this stress, depends on the dome's geometry and on the turbulence intensity of the approaching flow. The dependence of the gust effect factor on these parameters was investigated, based on a series of quasi-static analysis for a wide range of the dome's geometry.
- (5) Empirical formulas were provided for the gust effect factor and the equivalent pressure coefficients, which reproduces the same load effects as that the practical pressure distribution induces. The validity of these formulas was confirmed by comparing the maximum load effects predicted by the formula with those obtained from the quasi-static analysis. Using these formulas, we can easily estimate the design wind loads with an allowable error, despite the simple model.

## Acknowledgements

The authors would like to thank Messrs. M. Suzuki and T. Tsuchiya of Kajima Technical Research Institute for help with the wind tunnel experiments. They also are indebted to Messrs. A. Sasaki and O. Kuribara, former graduate students of Tohoku University, for their assistance with the computer programs and to Miss. M. Noguchi, a graduate student of Tohoku University, for her help with the data processing.

## References

- Architectural Institute of Japan (1993), *Recommendations for Loads on Buildings* (in Japanese; the English version was published in 1996).
- Davenport, A.G., Surry, D. and Stathopoulos, T. (1977), "Wind loads on low-rise buildings: final report of phase I and II", *Engineering Science Report BLWT-SS8*, University of Western Ontario.
- Davenport, A.G. and Surry, D. (1984), "Turbulent wind forces on a large span roof and their representation by equivalent static loads", *Canadian J. Civ. Eng.*, **11**, 955-966.

- Jeong, S.-H., Bienkiewics, B. and Ham, H.-J. (2000), "Proper orthogonal decomposition of building wind pressure specified at non-uniformly distributed pressure taps", *J. Wind Eng. Ind. Aerod.*, **87**, 1-14.
- Fukushi, M., Kikuchi, M., Uematsu, Y. and Yamada, M. (1991), "Characteristics of the wind loads on spherical domes - Part 1 Time-averaged wind pressure -", *Summaries of Technical Papers of Annual Meeting*, Architectural Institute of Japan, Structures I, 191-192 (in Japanese).
- Hongo, T. (1995), "Experimental study of wind forces on spherical roofs", Ph.D. Thesis, Tohoku University, (in Japanese).
- Letchford, C.W. and Sarkar, P.P. (2000), "Mean and fluctuating wind loads on rough and smooth parabolic domes", *J. Wind Eng. Ind. Aerod.*, **88**, 101-117.
- Liu, J., Xue, S. and Yamada, M. (1996), "Comparison between experimental result and numerical analysis for dynamic response of a single-layer latticed dome", *Proceedings of Asia-Pacific Conference on Shell and Spatial Structures*, Beijing, P.R. China, 668-673.
- Mataki, Y., Iwasa, Y., Fukao, Y. and Okada, A. (1988), "Wind induced response of low-profile cable-reinforced, air-supported structures", *J. Wind Eng. Ind. Aerod.*, **29**, 253-262.
- Nakayama, M., Sasaki, Y., Masuda, K. and Ogawa, T. (1998), "An efficient method for selection of vibration modes contributory to wind response on dome-like roofs", *J. Wind Eng. Ind. Aerod.*, **73**, 31-44.
- Ogawa, T., Nakayama, M. and Murayama, S. (1988), "Characteristics of wind pressure on spherical domes in turbulent boundary layers", *Proceedings of the 10th National Symposium on Wind Engineering*, Tokyo, Japan, 55-60 (in Japanese).
- Ogawa, T., Nakayama, M. and Murayama, S. (1989), "Characteristics of wind pressure on spherical domes and response of domes in turbulent flow", *J. Struct. Constr. Eng.*, Architectural Institute of Japan, **404**, 95-102 (in Japanese).
- Suzuki, Y., Kiya, M., Sampo, T. and Naka, Y. (1987), "Pressure fluctuations on the surface of a hemisphere immersed in a thick turbulent boundary layer", *J. Fluid Eng.*, Transaction of the ASME, **109**, 130-135.
- Taniguchi, T., Taniike, Y. and Nishimura, H. (1996), "POD analysis with weighted-area and time-lag for pressures on spherical roof", *Proceedings of the 14th National Symposium on Wind Engineering*, Tokyo, Japan, 323-328 (in Japanese).
- Uematsu, Y., Yamada, M. and Fukushi, M. (1994), "Structural characteristics and wind-induced dynamic behavior of a long-span spherical dome", *Interactions of Fluids, Structures and Mechanics, Proceedings of 12th Symposium on Engineering Applications of Mechanics*, Montreal, Canada, 127-136.
- Uematsu, Y., Yamada, M., Inoue, A. and Hongo, T. (1997), "Wind loads and wind-induced dynamic behavior of a single-layer latticed dome", *J. Wind Eng. Ind. Aerod.*, **66**, 227-248.
- Uematsu, Y., Kuribara, O., Yamada, M. and Hongo, T. (2001a), "Wind-induced dynamic response of a single-layer latticed dome", *Proceedings of International Symposium on Theory, Design and Realization of Shell and Spatial Structures*, Nagoya, Japan (CD-ROM).
- Uematsu, Y., Sone, T., Kuribara, O. and Yamada, M. (2001b), "Wind-induced dynamic response and its load estimation of an elliptic dome", *Proceedings of International Symposium on Theory, Design and Realization of Shell and Spatial Structures*, Nagoya, Japan (CD-ROM).
- Uematsu, Y. and Yamada, M. (2002a), "Wind-induced dynamic response and its load estimation for structural frames of circular flat roofs with long spans", *Wind Struct., An Int. J.*, **5**(1), 49-60.
- Uematsu, Y., Kuribara, O., Yamada, M., Sasaki, A. and Hongo, T. (2002b), "Wind-induced dynamic behavior and its load estimation of a single-layer latticed dome with a long span", *J. Wind Eng. Ind. Aerod.*, **89**, 1671-1687.
- Yamada, M. (1984), "An approximation on the buckling analysis of orthogonally stiffened and framed spherical shells under external pressure", *Shell and Spatial Structures Engineering*, Pentech Press, London, 177-193.
- Yamada, M. and Ishikawa, T. (1987), "Buckling of rigidly jointed single layer latticed spherical shells under external pressure", *Proceedings of the International Colloquium on Space Structures for Sports Buildings*, Beijing, China, 353-360.